Atmósfera (1991), **4**, pp. 117-138

A numerical study of warm cloud interactions

RAQUEL V. FRANCISCO, JOSEFA C. MONDARES

Philippine Atmospheric, Geophysical and Astronomical Services Administration (PAGASA), Quezon City, Philippines

MARIANO A. ESTOQUE

Visiting Professor, Department of Meteorology and Oceanography, Quezon City, University of the Philippines

(Manuscript received April 24, 1990; accepted in final form October 25, 1990)

RESUMEN

Se presenta un modelo de nubes en dos dimensiones, incluyendo en detalle procesos microfísicos. Representando un espectro desde 1 μm a 4 mm de radio, las gotas de agua se clasificaron en 37 categorías de acuerdo a su tamaño. El número de gotas de agua en cada categoría es una función de los procesos de colección y condensación. El proceso de nucleación originó nuevas gotas de agua.

Los resultados muestran que el modelo es capaz de simular el ciclo de vida de nubes calientes desde sus etapas iniciales hasta su disipación. Para iniciar la convección en el modelo, se usó una perturbación caliente y húmeda. La perturbación usada tuvo por características: 1 kilómetro de ancho, 1 kilómetro de profundidad y base a 800 metros de altura. Las observaciones de nubes obtenidas el Día 261 de 1974 durante el experimento GATE permitieron comprobar que el modelo reproduce razonablemente bien las características de dichas nubes.

Los experimentos numéricos de la interacción de dos nubes muestran que, cuando prevalece calma como condición inicial, dichas dos nubes se unen formando una sola. No ocurre unificación en presencia de flujo con cizallamiento como condición inicial.

Cuando se introdujeron simultáneamente dos perturbaciones iniciales en un flujo básico con cizallamiento, se observó que, de las dos perturbaciones, aquélla relativamente localizada en la dirección opuesta a la del vector cizallamiento se desarrolla más intensamente. Esta intensa perturbación es más intensa que la obtenida en el experimento de sólo una perturbación inicial. Cuando la segunda perturbación se introduce 15 minutos después de la primera, la célula más reciente se desarrolla más vigorosamente mientras que la célula vieja se disipa. la duración de vida es más larga y la precipitación es más intensa cuando la posición de la nueva célula con respecto a la vieja está en dirección opuesta a la del vector cizallamiento.

La formación de lluvia en la simulación producida en el modelo es bastante rápida; la lluvia duró entre 10 y 15 minutos, aproximadamente. Ese hecho se atribuyó al uso del un perfil de temperatura y humedad del tipo "top-hat" como condición inicial así como en el uso detallado de los procesos microfísicos en el mundo.

ABSTRACT

A two-dimensional, slab-symmetric cloud model with detailed microphysics is presented. Drops were classified into 37 size classes representing a droplet spectrum from 1 μm to 4 mm radius. Each class of droplet was subjected to condensation and collection processes. New droplets were formed by the nucleation process.

Results show that the model is capable of simulating the life history of a warm cloud from the initiation to the dissipation stages. A warm, moist perturbation or impulse, 1 km wide and 1 km deep with base at 800 m, is used to trigger convection in the model. Comparison of our study on isolated clouds with actual observations based on Day 261 of GATE reveal some realistic features of the model.

Numerical experiments on cloud interactions show that merging occurs when a calm environment is initially used. No merging occurs when a sheared flow is incorporated in the model. When the two impulses are introduced simultaneously, the upshear cell develops more strongly compared with an isolated cell or its downshear counterpart. The growth of the downshear cell seems suppressed. When the second impulse is introduced 15 minutes later, the newer cell develops more vigorously while the older cell dissipates. The lifetime is longer and the rainfall heavier when the new cell is located upshear of the older cell.

The formation of rainfall from the simulation is quite rapid; the rainfall lasted for about 10 to 15 minutes. This feature is attributed to the use of a top-hat profile of the temperature and humidity for triggering initially the cloud growth and to the use of detailed microphysics in the model.

1. Introduction

Cloud interactions are important processes in the development of cumulus cloud systems. They exist if the development of at least one cell in a group of clouds is not the same as when it is isolated. Through dynamical and physical processes, these interactions lead to either an invigorated or weakened cloud, merged or farther separated clouds, suppressed or added new cell growth.

Various observational investigations have been made on cloud interactions. One of the first of such investigations was done by Byers and Braham (1949). In their investigations of multiple-cell radar echoes on Florida and Ohio storms, they noted preferred new cell growth adjacent to existing cells less than 6 miles (9.6 km) apart over new growth at a distance greater than 9 mi (14.5 km). They also found that new echoes were most likely to form between the cells than at any other areas.

Merging was observed by Byers and Braham (1949) as another outcome of cloud interactions. This was indicated by the merging of the radar echoes of two cells in the 9 July 1946 case study of a Florida storm. Merging was confirmed by Malkus (1954) when she observed that several updrafts near cloud base (665 m) appeared to join at higher levels to form a single updraft. From collaborating visual observations, she noted that below 830 m, intermittent clear air pockets extending to cloud base were visible. It was postulated that such middle-sized cumuli were formed from the aggregation of several smaller ones.

In succeeding radar studies, mergers were defined as occurring when separate echoes join at a given detectable reflectivity signal (Lopez, 1976; Westcott, 1977). Their studies indicated that merging resulted in a larger, more organized system that produced more rainfall. They concluded that development of more intense reflectivity cores is favored because of mutual protection of the cells from dilution by the drier evironment.

Simpson (1980) proposed merging to be caused by cumulus downdrafts and associated cold outflows. This interaction enhances low level convergence and triggers new cell growth between two cloud masses that could be separated by some small (4 km) or sizeable (35 km) distance. Subsequently, this new cloud growth becomes a bridge between existing areas of convection.

Another type of cloud interaction observed by Byers and Brahan (1949), Scorer and Ludlam (1953) and Malkus (1954) involves the development of successive turrets. One cell eventually is replaced by another in the same location. It was hypothesized that the predecessors "wet" the environment, thereby causing the successors to grow taller.

Turpeinen and Yau (1981) presented evidence that clouds which lie close together exhibit mutual suppression. This appears to be in disagreement with the observations of Byers and Braham (1949) cited above. They analyzed 5 minute resolution Quadra data on day 261 of GATE in medium-

sized convective cells. They stratified their data according to minimum edge to edge separation (d) between cells: 1) isolated cells, $d > 7$ km; 2) relatively isolated cells, $2 < d < 7$ km; 3) cells close to another cell $0 < d < 2$ km; and 4) merging cells, $d = 0$ km. For a fixed interval of maximum area, the maximum reflectivity factor and echo top generally decrease with a decrease in edge to edge separation. Isolated cells are stronger and taller than comparable-sized cells lying close to another cell indicating a possible mutual suppressing mechanism in the latter case.

Other types of cloud interactions have been observed by Turpeinen (1982) and Turpeinen and Yau (1981). They found that in the merging of two cells, the upshear cell tends to be stronger in terms of maximum reflectivity factor than the other, especially if the clouds are simultaneous. For non-simultaneous cells, the downshear cell had a tendency to develop earlier than the upshear cell and also tended to dominate.

Radar observations have the capability to identify merging precipitation areas. However, dynamical and microphysical structures can only be implied but cannot be related directly with the radar echoes. The weakness in radar observations may be remedied by numerical modeling. Evidently, numerical modeling is an important method for investigating merging and also other types of cloud interactions. So far, only a few numerical studies have been performed to study cloud interactions and merging processes. Among the first studies is that by Wilkins *et al.* (1976) who used a two-dimensional model to study the effect of distance between two clouds. They found out that the velocity fields of the thermals interfere with each other resulting in a repulsion between two rising thermals. When the distance between the cells is close enough, merging occurs with a buoyancy twice that of a solitary cloud.

In a subsequent numerical study using a two-dimensional model, Orville *et al.* (1980) found that a pair of non-identical model clouds –one cloud stronger or 6 minutes older than the other– favor merging. The mechanism of merging was attributed to the existence of a pressure gradient directed from the weaker and younger cell toward the older and stronger one.

Turpeinen and Yau (1981) and Turpeinen (1982) developed the first three-dimensional model to study cloud interactions. Their model can adequately represent wind shear and air circulations. Their studies showed that the use of non-identical impulses does not seem to promote merging. Instead, their results indicated further substantial suppression of the weaker cloud as compared with a similar but isolated cloud. They attributed the suppression to the inner downdrafts forced to develop inside the cloud boundaries because of the circulation of the adjacent cell. Strong evaporation and mixing resulted in a decreasing buoyancy thus inhibiting the cloud development as a whole.

All of the above numerical studies use two thermal impulses in their initialization scheme. Tao and Simpson (1984) were the first to study the development of multiple cells in a two-dimensional, slab-symmetric model. Clouds are initially generated by large-scale lifting and random temperature perturbations. The results showed increased occurrences of cloud merger with increased intensity of large-scale lifting and atmospheric instability. In 14 cases of cloud mergers, they observed that the dominant merging mechanism is the cumulus downdraft and its associated cold outflow. The sequence of events of the cloud merging process was described as follows:

1) There is development of one or two cloud-scale downdrafts which are associated with two interacting clouds.

2) A visible cloud bridge which connects the interacting clouds forms near the cloud base. The

formation of the cloud bridge is evidence of a low-level convergence zone between the interacting clouds.

3) One or more new convective cells start to grow at the location of the bridge. The new generation of convection is primarily due to the effect of cloudscale downdrafts and their associated cold outflows.

4) The new cells develop vigorously through the enhancement of low level convergence. A dynamic merging process can occur between the new convection and one of the interacting clouds in some particular cases.

5) Successive generation of several newer convective cells can take place after the vigorous development of new convection. The larger and longer life history of the cloud system, thus, produces more precipitation.

Previous numerical studies on cloud interactions so far have used non-parameterized microphysics similar to Kessler's (1969) scheme. The liquid water content is represented by two classes: cloud droplets which move with the surrounding air flow, and precipitation raindrops. During the first International Cloud Modelling Workshop, it was found out that parameterized microphysics is insufficient for accurate representation of rainfall formation. Rainfall formation is an important aspect of cloud interactions. Therefore, one should study these interactions with models which incorporate microphysical processes more accurately. We have attempted to develop such a model for the purpose of studying the interactions of warm clouds. The model incorporates 37 classes of droplet sizes ranging from 1 μm to 4 mm radius. This paper describes the model in detail and presents the initial results of the use of the model to study warm cloud interactions.

2. The numerical model

The model is based primarily on similar models described by Orville (1965), Orville and Sloan (1970), Orville and Kopp (1977), Takeda (1971) and Hall (1980). It is a two-dimensional, slab-symmetric, anelastic model with detailed microphysics. As mentioned in the previous section, the model incorporates 37 classes of droplet sizes ranging from 1 μm to 4 mm radius. The formation and the growth of each droplet by condensation and coalescence are followed in detail. The detailed microphysics allows supersaturation to take place when the rate of condensation is slow relative to the excess vapor present. It also allows subsaturation where droplets are present when the rate of evaporation is not enough to saturate the environment. Consequently, the model should be able to predict the formation of precipitation more realistically.

Defining the vorticity as $\varsigma = \frac{\partial \rho_o w}{\partial x} - \frac{\partial \rho_o u}{\partial z}$, the following vorticity equation is used:

$$\frac{\partial \varsigma}{\partial t} = -u\frac{\partial \varsigma}{\partial x} - w\frac{\partial \varsigma}{\partial z} + 2w\frac{\partial \rho_o}{\rho_o \partial z}\left[\varsigma + u\frac{\partial \rho_o}{\partial z}\right]$$

$$-uw\frac{\partial^2 \rho_o}{\partial z^2} + \frac{\rho_o g}{T_{vo}}\frac{\partial T_v}{\partial x} - \rho g\frac{\partial \ell}{\partial x} + v\nabla^2\varsigma \qquad (1)$$

The first and second terms on the right hand side of (1) are the advection terms; the third and fourth terms represent the effect of the local incompressibility; the fifth term represents the

buoyancy force which is due to the horizontal variations of temperature; the sixth term represents the buoyancy force due to horizontal variations of liquid water; and the last term represents the effect of eddy diffusion. The use of the vorticity equation eliminates pressure as an explicit dependent variable.

It is assumed that the eddy diffusion coefficient is constant in both time and space. A value of 25 m^2 s^{-1} is used for v. This is the optimum value which has been chosen through numerical experimentation using different values of v.

Since the system is non-divergent and locally incompressible, the horizontal and vertical mass fluxes may be expressed in terms of a streamfunction, ψ. Thus:

$$\rho_o u = -\frac{\partial \psi}{\partial z} \tag{2}$$

$$\rho_o w = \frac{\partial \psi}{\partial x} \tag{3}$$

$$\zeta = \nabla^2 \psi = -\frac{\partial}{\partial z}(\rho_o u) + \frac{\partial}{\partial x}(\rho_o w) \tag{4}$$

The thermodynamic equation is based on the first law of thermodynamics and is given by:

$$\frac{\partial T}{\partial t} = -u\frac{\partial T}{\partial x} - w(\frac{\partial T}{\partial z} + \Gamma_d) + \frac{LC}{C_P} + v\nabla^2 T \tag{5}$$

The first and second terms on the right hand side are the advection of temperature, the third is the heating rate (positive during condensation and negative during evaporation) and the fourth term is the thermal eddy diffusion. The quantity, C, is the condensation or evaporation rate and is computed from the change of total liquid water content during the given time interval. When unsaturated air prevails and there are existing droplets, evaporation takes place. This leads to increase in vapor content and decrease in temperature. In this case, C refers to the amount of droplets evaporated.

The water vapor equation is represented by:

$$\frac{\partial q}{\partial t} = -u\frac{\partial q}{\partial x} - w\frac{\partial q}{\partial z} - C + v\nabla^2 q \tag{6}$$

The time rate of change of the number (N) of water drops with radius r per unit volume is based on Hall (1980):

$$\frac{\partial N}{\partial t} = \frac{\partial \eta}{\partial t} - \frac{\partial}{\partial r}(N\frac{Dr}{Dt}) - u\frac{\partial N}{\partial x} - w\frac{\partial N}{\partial z} + \frac{\partial}{\partial z}(NV_T) + v\nabla^2 N$$

$$+\frac{1}{2}\int_{v'=0}^{v} N(v-v',\ t)N(v',\ t)K(v',\ v-v')dv'$$

$$-N(v,\ t)\int_{v'=0}^{v_{\max}} N(v',\ t)K(v,\ v')dv' \tag{7}$$

The first term on the right hand side represents the effect of cloud condensation nuclei, the second term represents the effect of condensation, the third and fourth terms are the advection terms, the fifth term represents the fallout term, the sixth term is the effect of diffusion, the seventh term represents the increase of droplets of volume v that have formed by the coalescence of droplets of volumes $(v - v')$ and v' and the last term represents the loss of droplets of volume v due to its coalescence with the entire droplet spectrum. Breakup of droplets is not included.

The concentration of activated cloud condensation nuclei (CCN) increases with increasing supersaturation. This behavior is parameterized in the form (Hall, 1980):

$$\eta^* = cS^K \tag{8}$$

where η^* is the number concentration of activated condensation nuclei, S is supersaturation, K and c are assumed to be constant. On the basis of observations of maritime air, $K \approx 0.7$, $c \approx 100$ cm^{-3} (Pruppacher and Klett, 1980).

It is assumed that activation occurs instantaneously as the supersaturation changes and only droplets of critical size are produced. Thus:

$$\left[\frac{\partial N}{\partial t}\right]_{x_1} |_{\text{nucleation}} = \frac{1}{\Delta t}\Delta\eta \tag{9}$$

where $\Delta\eta$ is the positive difference between η^* and the number of previously active nuclei per unit volume of air. It is set to 0 if the value of $\Delta\eta$ is negative.

The equation for condensation rate of a droplet of radius r is based on Takeda (1971).

$$\frac{Dr}{Dt} = \frac{\frac{1}{r\rho_w}\left[S - \frac{a}{r}\right]f}{\frac{L^2}{R_v T^2 k} + \frac{R_v T}{De_s}} \tag{10}$$

where S is the supersaturation and is defined as $S = \frac{q_v}{q_{vs}} - 1$.

The effects of surface tension a and the ventilation factor f are expressed as follows (Takeda, 1971):

$$a = \frac{2\sigma\varepsilon}{\rho_w R_v T^2} \tag{11}$$

$$f = 1 + 0.225 Re^{1/2} \tag{12}$$

The surface tension, σ, is calculated from $\sigma = 76.1 - 0.155T$. The symbol ε represents the ratio of the molecular weight of water to molecular weight of dry air and is approximately equal to 0.622. The Reynolds number, Re, is computed from $Re = 14.14 r V_T$ where V_T is the terminal velocity of a droplet of radius r.

The latent heat of vaporization L is computed from:

$$L = 3.150 \times 10^{10} - 2.376 \times 10^7 T \tag{13}$$

This formula is line of best fit on experimental values within the interval -40°C to 40°C.

The formula for computing saturation vapor pressure e_s is the same one used by Orville (1965):

$$e_s = 6.11\left[10^{7.5\{\frac{T-273}{T-36}\}}\right] \tag{14}$$

Assuming that the cloud is homogeneous, the collection kernel $K(v, v')$ in Equation (7), defined as the coalescence rate of droplets of volumes v and v', is:

$$K(v,\ v') = \pi(r + r')^2 E(r,\ r') \mid V_T(r) - V_T(r') \mid \tag{15}$$

where $E(r, r')$ is the collection efficiency of two interacting droplets and is equal to the product of collision and coalescence efficiencies; $\mid V_T(r) - V_T(r') \mid$ is the absolute value of the difference of the terminal speeds of the droplets of volume v and v'; and $\pi(r + r')^2 \mid V_T(r) - V_T(r') \mid$ is the volume during a unit time through which a droplet of radius r sweeps out droplets of radii r'. The collision efficiencies have been used previously by Takahashi (1981). These were furnished to the authors by him.

The droplets spectrum is discretized onto a logarithmic radius grid with mass doubling for every grid interval. The radius and mass of each interval are:

$$r(J) = r_o 2^{(J-1)/3} \tag{16}$$

$$x(J) = x_o 2^{(J-1)} \tag{17}$$

where $J = 1, 2, \ldots, J_{\max}$. $J_{\max}$ is the number of size classes desired which is 37. The smallest radius considered, r_o, is equal to 1 μm. The maximum value $r(37)$ corresponds to a droplet of radius of 4096 μm.

The stochastic coalescence terms in Eq. (7) can be expressed as:

$$\frac{\partial}{\partial t}N(J_{x+y}) = \sum_{J_y=1}^{J_{\max}} \sum_{J_x=1}^{J_y} K(J_x,\ J_y)N(J_x)N(J_y)$$

$$- \sum_{J=1}^{J_{\max}} K(J_{x+y},\ J)N(J_{x+y})N(J) \tag{18}$$

The first term on the right hand side of (18) represents the increase in number of droplets of mass $x + y$ due to drops of mass y coalescing with drops of mass x. The second term represents the loss of droplets of mass $x + y$ due to their coalescing with other drops. Since droplets of mass $x + y$ may fall between the central values of two adjacent classes, they are distributed into these two classes using the redistribution factor $R(J, J')$ defined as

$$R(J,\ J') = \begin{cases} \frac{x'(J)-x(J-1)}{x(J)-x(J-1)}, & x(J-1) < x'(J) < x(J) \\ \frac{x(J+1)-x'(J')}{x(J+1)-x(J)}, & x(J) < x'(J) < x(J+1) \\ 0 \quad , & \text{otherwise} \end{cases} \tag{19}$$

let $x' = x+y$ such that $x'(J')$ is between $x(J)$ and $x(J+1)$, the new $N^*(J)$ at $t+1$ is computed from $N(J')$ as follows:

$$N^*(J) = \sum_{J'=1}^{J} R(J,\ J')N(J') \tag{20}$$

This method conserves mass and number of droplets.

The terminal velocities in cm s^{-1} for various drops sizes are:

$$V_T = 1.26 \times 10^6 r^2, \qquad r < 40\mu m \tag{21}$$

$$V_T = 8000r, \qquad 40\mu m \leq r < 500\mu m \tag{22}$$

$$V_T = 1400(2r)^{1/2}, \qquad r \geq 500\mu m \tag{23}$$

(21) is the Stoke's Equation while (22) and (23) are by Gunn and Kinzer (1949).

3. Initial conditions, boundary conditions and numerical schemes

The data used in the study represent trade wind conditions which correspond to the 1200 GMT sounding of Day 261 (18 Sep 1974) of GATE (the Atlantic Tropical Experiment of the Global Atmospheric Research Program, centered in an area near 8°N, 23°W) shown in Fig. 1.

The temperature profile is almost dry adiabatic in the first 600 m above ground, conditionally unstable between 600 and 1000 m and moist adiabatic between 100 and 1650 m. A stable layer is found between 2 and 2.8 km.

The moisture profile shows a relatively moist layer from the ground up to 2.2 km, followed by a dry layer above this level up to 3.4 km.

Fig. 2 shows the wind profile used in the model. The same profile was used in the study of Turpeinen and Yau (1981). At lower heights, the flow is southerly, becoming northerly as height increases.

To trigger convection, this study used a thermally buoyant, saturated perturbation 1 km wide and 1 km deep, the base of which is 800 m above the surface. Its temperature is warmer by 0.5°C with respect to the environment and its relative humidity is 100%. There is no updraft initially. Convection is triggered by thermal buoyancy.

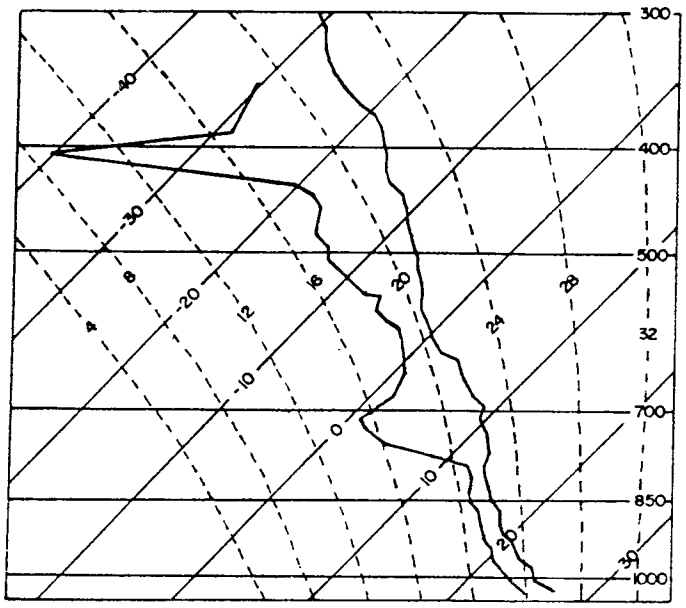

Fig. 1. Soundig made at 1200 GMT Day 261 of GATE plotted on a skew T log P thermodiagram.

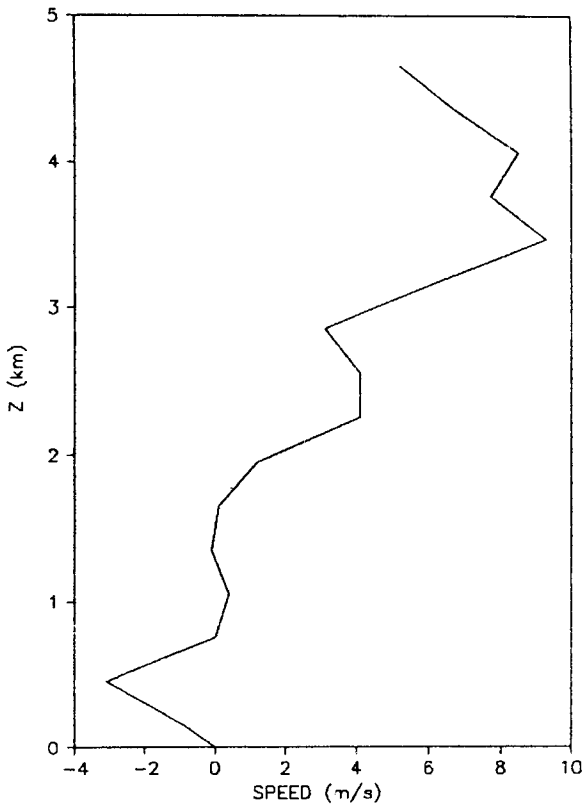

Fig. 2. Initial wind (N-S component).

The domain is 10 km in the horizontal and 6 km in the vertical; there are 51×31 grid points, each separated by a distance of 200 m.

The boundary conditions in the vertical are free slip with no mass flux across these surfaces:

$$w = 0, \ \zeta = 0 \qquad \text{at } z = 0 \text{ and } z = z_n \tag{24}$$

The boundary conditions of T and q at the top are:

$$\frac{\partial T}{\partial t}, \qquad \frac{\partial q}{\partial t} = 0 \qquad \text{at } z = z_n \tag{25}$$

At the ground:

$$\left[\frac{\partial T}{\partial x}\right]_{z=z_o} = \left[\frac{\partial T}{\partial x}\right]_{z=z_1} \tag{26}$$

$$\left[\frac{\partial q}{\partial x}\right]_{z=z_o} = \left[\frac{\partial q}{\partial x}\right]_{z=z_1} \tag{27}$$

The variables at the lateral boundaries change with time, depending whether there is inflow or outflow. For outflow and no flow, the horizontal gradients of T, q and N are assumed to be uniform at the boundaries. Thus:

$$\frac{\partial^2}{\partial x^2}(T, \ q, \ N) = 0 \qquad \text{at } x = x_L \text{ and } x = x_R \tag{28}$$

In the case of inflow, horizontal gradiente of T, q and N are assumed to be 0:

$$\frac{\partial}{\partial x}(T, \ q, \ N) = 0 \qquad \text{at } x = x_L \text{ and } x = x_R \tag{29}$$

For the numerical integration of the differential equations the forward differencing scheme in time and the forward upstream differencing scheme in space for advection terms are used. The centered differencing scheme is used for non-advection terms.

4. Numerical experiments

In order to investigate cloud interactions, we made six integrations of the model (called experiments). A total of six experiments are included in this investigation. Two of these are single cloud experiments (Sc and Ss) while the remaining four are double cloud experiments (Dc, Ds1, Ds2 and Ds3). The letter S denotes single-cloud experiments and the letter D denotes double-cloud experiments. The small letters c and s denote experiments using calm and sheared environment, respectively.

The single cloud experiments serve primarily as bases for determining the effects of cloud interactions. This is done by comparing them with the appropriate double cloud experiments. For example, for the purpose of determining the effects of cloud interaction in a calm environment, one should compare Experiment Sc with Experiment Dc.

Table I. Parameters of the experiments using Day 261 of GATE data.

Experiment	Wind shear ($v_{3450} - v - 450$) (m s^{-1})	Number of impulses	Distance between impulses (km)	Time between impulses (min)
Sc	0	1	–	–
Ss	11.6	1	–	–
Dc	0	2	1	0
Ds1	11.6	2	1	0
Ds2	11.6	2	2	15 (upshear cloud first)
Ds3	11.6	2	2	15 (downshear cloud first)

The characteristics of the experiments are summarized in Table I. The wind shear is expressed as the maximum difference in horizontal velocity with height. This was found to be 11.6 m s^{-1} which is the difference between winds at 3450 and 450 m height.

Double cloud experiments include simultaneous cases under initial calm atmospheric conditions (Dc) and sheared surroundings (Ds1). Non-simultaneous experiments are done under sheared environment with either the upshear cloud (Ds2) or the downshear cloud (Ds3) initiated 15 minutes earlier.

5. Results

5.1. Isolated Clouds

The results of Experiment Sc are shown in Fig. 3 which shows the cloud development after 10, 20, 25 and 30 minutes of integration time. The cloud outline is depicted arbitrarily by the 0.1 g m^{-3} contour of LWC.

The following thermal, dynamical and microphysical features are observed:

(1) After 10 minutes of integration time, the initial impulse develops into a cloud with a diamenter of 1.4 km and a cloud top height of 2.2 km. The maximum LWC reaches 2.1 g m^{-3}. The maximum updraft occurs near the cloud center and has a value of 3.3 m s^{-1}. Note that the outflow is restricted to the upper portion of the cloud while inflow dominates the lower portion of the cloud. A double vortex is formed similarly to the results of Turpeinen and Yau (1981).

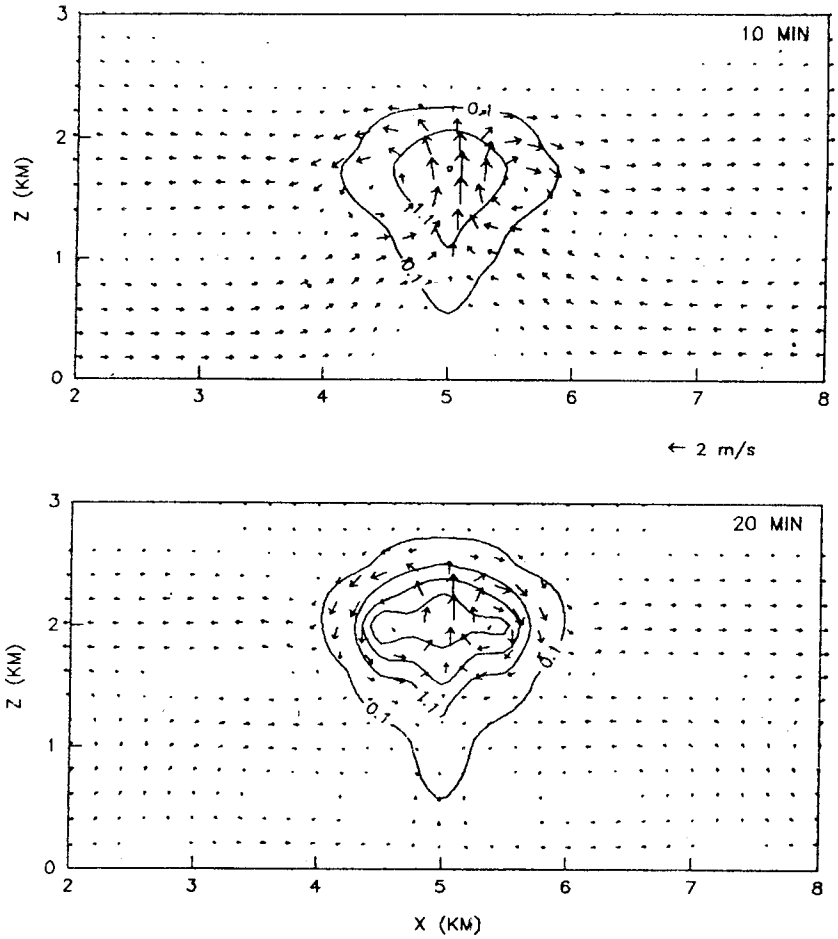

Fig. 3a. Wind and LWC fields of Experiment Sc at 10 and 20 minutes. Contour interval of LWC field is 1.0 g m^{-3}.

The growing cloud has a temperature excess as high as 1.22°C from the initial state (not shown). The warming is due to the release of latent heat of condensation. On the other hand, a cold dome is formed just above the cloud top and is due to the adiabatic lifting of unsaturated air and evaporation of droplets advected into this area.

(2) After 20 minutes of integration time, the cloud has grown larger with a diameter of 1.8 km and cloud top height of 2.4 km. The maximum LWC as shown in Fig. 3a is slightly above 3 g m^{-3}. This value is somewhat greater than those indicated by observations for cumulus clouds similar to our simulated clouds. However, in clouds under sheared flow (to be described later), the maximum LWC is smaller. The maximum updraft is lower than that at 10 minutes with a value of 3.0 m s^{-1}. Downdrafts occupy a wider area inside the cloud compared with the same cloud 10 minutes earlier. Convection at the lower layer is now weak.

(3) A precipitating cloud is developed at 25 minutes. Downdrafts prevail inside the cloud and reach a peak value of -2.0 m s^{-1}. The LWC maximum is reduced to 3.2 g m^{-3}. At 30 minutes, only a trace of cloud is left. Further integration in time leads to complete disappearance of cloud.

When the wind field is included in the initialization (Experiment Ss), the cloud tilts downshear, spreading more horizontally with time. At 25 minutes of cloud lifetime (Fig. 4), a downdraft

develops downwind but no rain falls, unlike Case Sc which precipitated at 25 minutes. At this time, the maximum LWC is a little in excess of 1 g m^{-3}. The maximum amount of rain that fell under sheared surroundings was only 0.3 mm which fell at $x = 6.2$ km, while that of case Sc was 2.5 mm. The wind shear effect on cloud development shown by this experiment is in agreement with observations.

The results of the two experiments on isolated clouds just described are quite realistic. In particular, the cloud top height of 2.4 km and the lifetime of 35 minutes are entirely reasonable on the basis of GATE observations (Turpeinen and Yau, 1981). We are, therefore, confident that the model could be used to study cloud interactions.

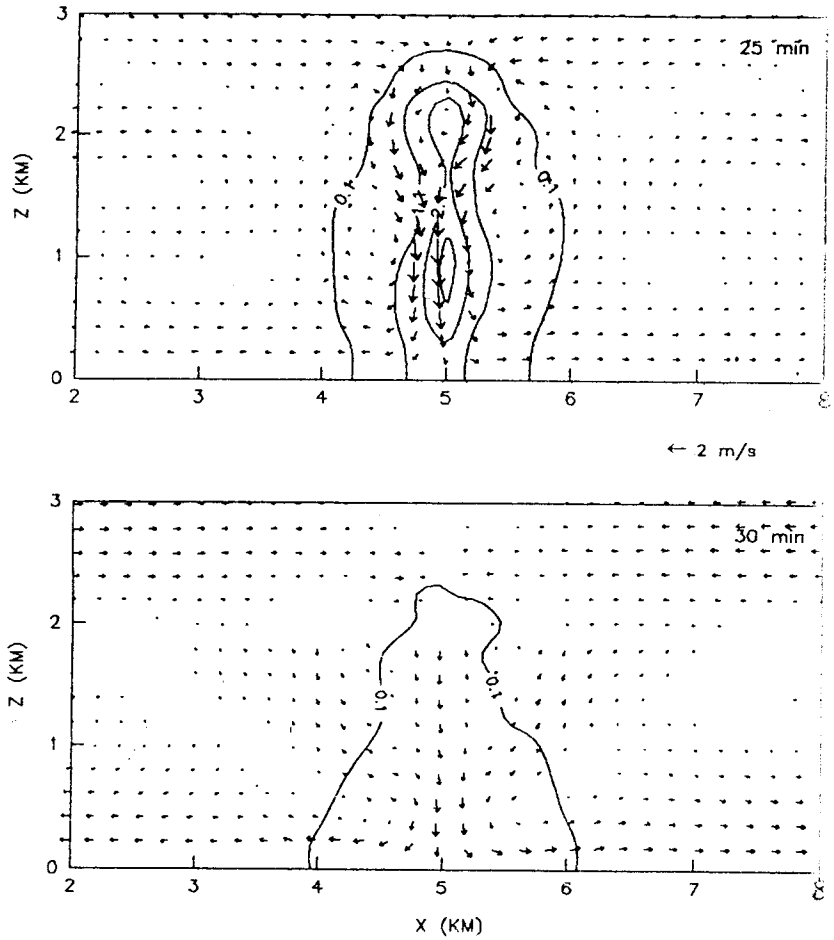

Fig. 3b. Wind and LWC fields of Experiment Sc at 25 and 30 minutes. Contour interval of LWC field is 1.0 g m^{-3}.

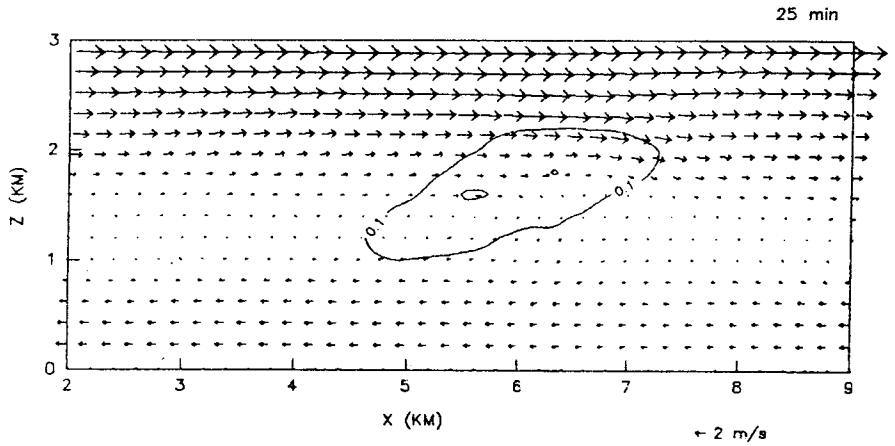

Fig. 4. Wind and LWC fields of Experiment Ss at 25 minutes. Contour interval of LWC field is 1.0 g m^{-3}.

5.2. Double clouds (interactions)

Next, we describe the experiments which involve double cloud cells. The first of these (Case Dc) represents the interaction of two impulses under calm environment. The results of the integration for this case are shown in Fig. 5. The initial cells were centered at $x = 4$ and $x = 6$ km. Their inner edges are 1 km apart. These cells started simultaneously.

It may be seen in Fig. 5a that a cloud bridge is formed between the cells after 33.5 min. In this connection, Simpson *et al.* (1971) observed that a cloud bridge always precede the merging process. The cloud bridge also appeared in the simulation experiment in a calm atmosphere by Turpeinen (1982). According to them, the bridge could be caused by the use of the overlapping initial impulses. The non-symmetric feature of our results is presumably due to the corresponding nonsymmetry in the numerical integration procedure used.

The updraft between the cells widens until complete merging occurs at 35 minutes as shown in Fig. 5b. Heavy rainfall develops rapidly at this merged area. The strong downdraft accompanying the heavy rainfall results in outflow near the ground. Thus, there is spreading out of rain.

In brief, the simulation of two impulses under initial calm conditions indicates that merging occurs. Fig. 6 shows the effect of merging on rainfall. Rainfall is increased three times in the merged case with respect to its single cloud counterpart.

The effect of including vertical windshear is demonstrated in Case Ds. The initial conditions used were the same as in the above case except that the vertical windshear is included. Fig. 7 shows the results of this experiment. A mild updraft develops between the cells at 10 minutes (Fig. 7a). Inflow of air is evident from the lower portion of the downshear cell towards the upshear cell. Subsequently, the upshear cell grows more vigorous than its downshear conterpart (Fig. 7b). This growth is in agreement with the results of the statistical study of Turpeinen and Yau (1981) on radar echoes on Day 261 of GATE. Their results suggest that the northern, upshear cell tend to be stronger for simultaneous cells. The suppression of the downshear cell was attributed by Turpeinen and Yau to the fact that the downshear cell is more exposed to the eroding effects of the inflow of the drier ambient air. Comparing with Case Dc, it is clear that the wind shear inhibits the growth of the cell.

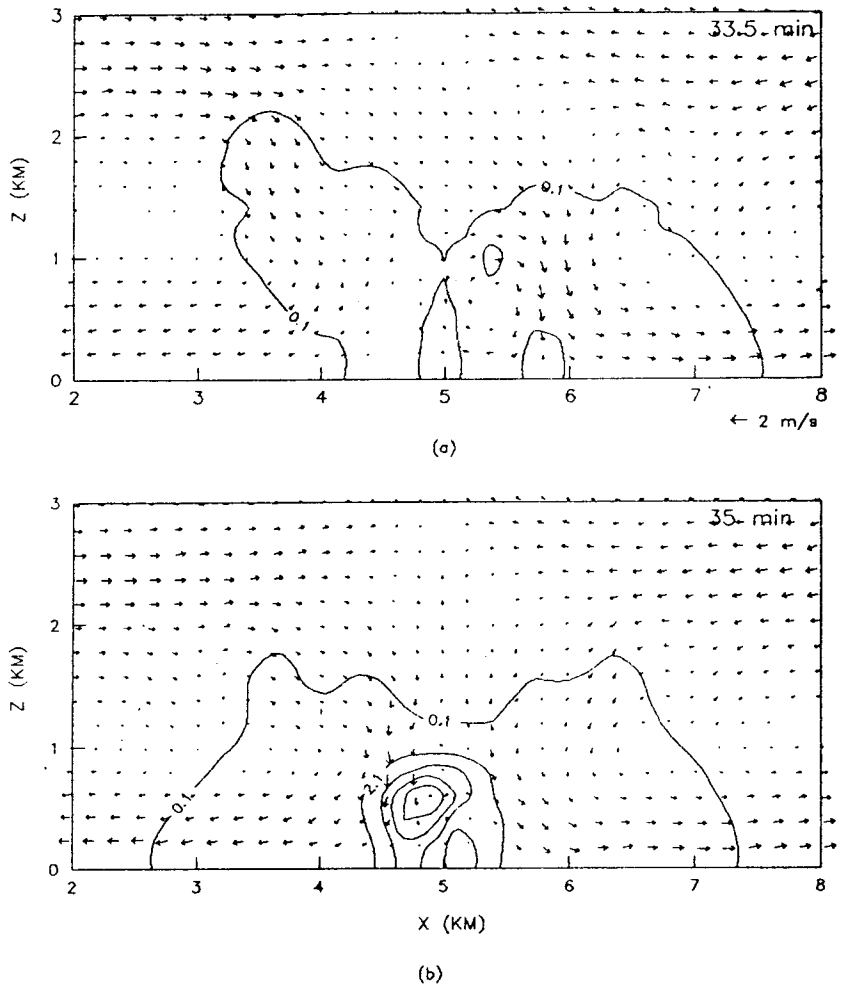

Fig. 5. Wind and LWC fields of Experiment Dc at 33.5 minutes and 35 minutes. Contour interval of LWC field is 1.0 g m^{-3} for (a) and 2.0 g m^{-3} for (b).

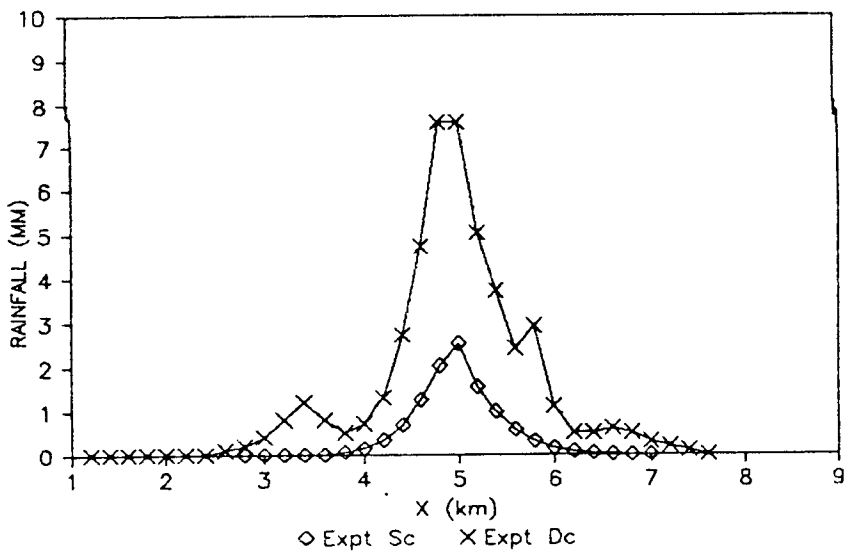

Fig. 6. Accumumulated rainfall of Experiments Sc and Dc.

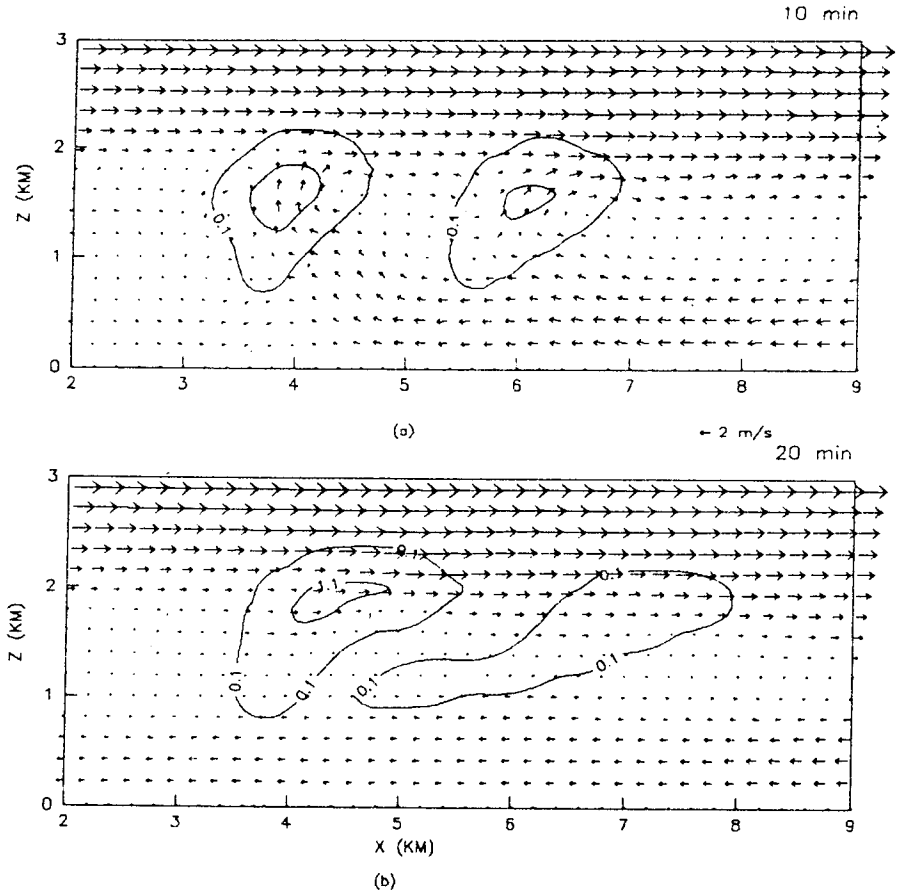

Fig. 7. Wind and LWC fields of Experiment Ds at 10 and 20 minutes. Contour interval of LWC field is 1.0 g m $^{-3}$.

Fig. 8 shows the effect of cloud interaction under sheared surroundings on rainfall. Experiment Ds1 produced a maximum rainfall of 0.7 mm at $X = 5.2$ km while that of Ss is only 0.3 mm at $X = 6.2$ km. At the same horizontal distance of 6.2 km, no rain fell from Ds1, a clear indication that the donwshear cell is indeed suppressed. On the other hand, the upshear cell is more vigorous than when it is isolated. The maximum rainfall is more than twice in Ds1 than in Ss.

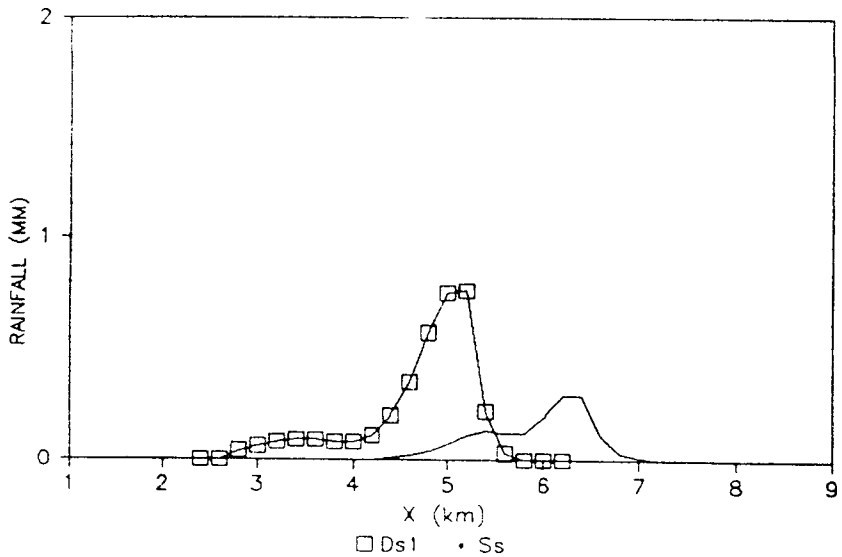

Fig. 8. Accumulated rainfall of Experiments Ss and Ds1.

Fig. 9 illustrates the simulation results when the second impulse is introduced downshear 15 minutes later (Experiment Ds2). It may be noted that in the previous experiment (Ds1) the initial impulses were simultaneous. The outflow air underrunning from the dissipating upshear cloud and the southerly flow into the downshear cell leads to updraft and further growth of this downshear cell. At 35 minutes the cloud is precipitating.

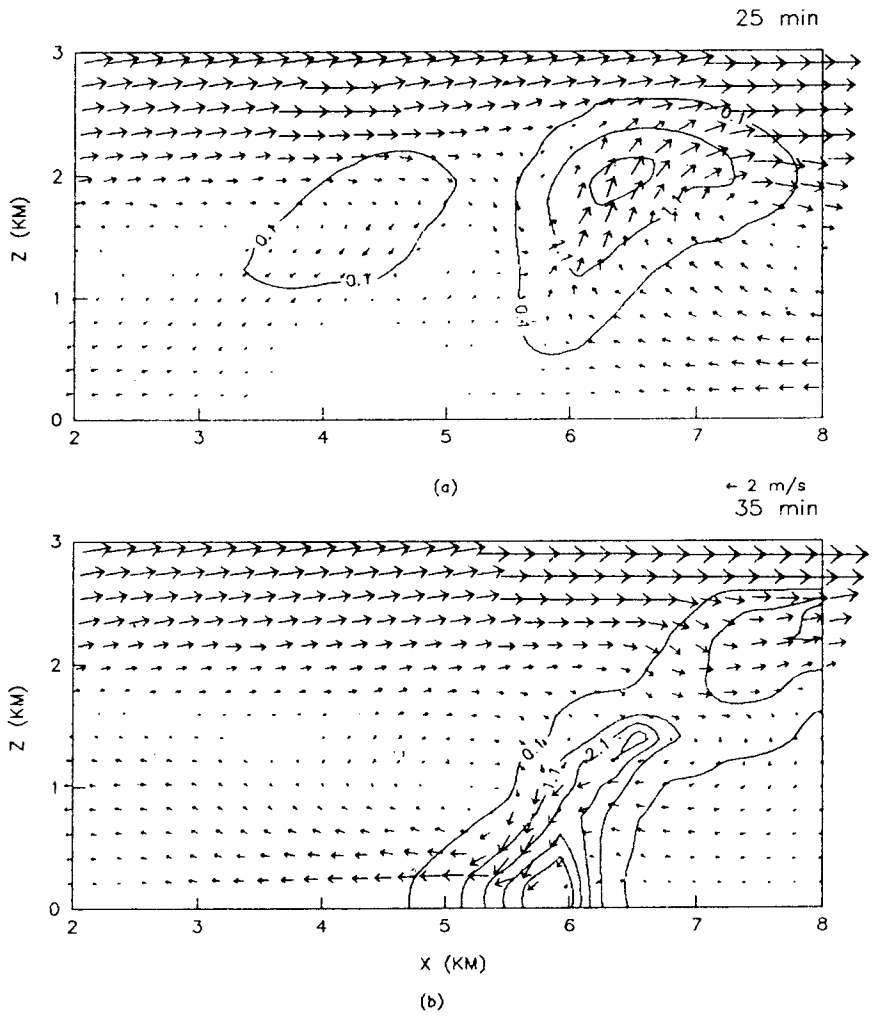

Fig. 9. Wind and LWC fields of Experiment Ds2 at 25 and 35 minutes. Contour interval of LWC field is 1.0 g m^{-3}.

In Fig. 10 (Esperiment Ds3), the downshear impulse was initiated 15 minutes before another initial impulse is introduced upshear. At 25 minutes (Fig. 10a), it may be seen that the new cloud has grown at the expense of the older cloud. The older, downshear cell is dominated by downdraft which feeds the upshear cell. Rainfall with a wider areal coverage than the previous case has occurred at 40 minutes. Compared with Experiment Ds2, this case exhibits more vigorous growth of the newer, upshear cell and heavier rainfall (Fig. 11). According to the study of Turpeinen (1982), when the downshear cell is first to develop, it becomes stronger than the younger, upshear cell. It may be mentioned that there were only 4 pairs of cells observed falling under this category. Only two out of four pairs demonstrated that the downshear cell became

stronger than the upshear cell. The other two cells had approximately equal maximum reflectivity factor. Thus, the observation is not conclusive.

In summary, the important findings of our simulations are as follows:

(1) Experiments Sc and Ss show that strong vertical wind shear is unfavorable for cumulus cloud development. This finding is also supported by Experiments Dc and Ds.

(2) Merging occurred when two impulses were initiated simultaneously in a calm atmosphere. Merging did not occur when sheared flow was introduced.

(3) When the impulses are introduced simultaneously in sheared flow, the upshear cell grows while the downshear cell dissipates. The maximum rainfall produced is 0.7 mm at $X = 5.2$ km.

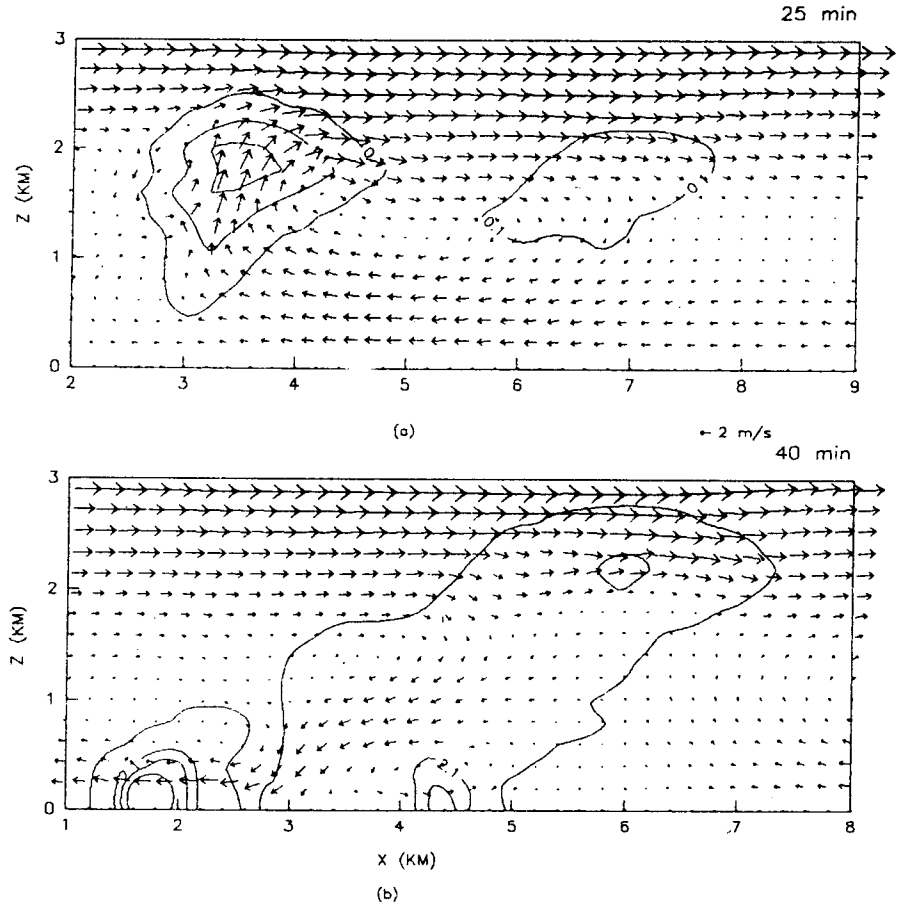

Fig. 10. Wind and LWC fields of Experiment Ds3 at 25 and 40 minutes. Contour interval of LWC field is 1.0 g m^{-3} for (a) and 2.0 g m^{-3} for (b).

(4) When the second impulse is introduced 15 minutes after the first impulse, this second cell, irrespective whether it is located upshear or downshear, grows more vigorously than the older cell.

(5) If the second impulse mentioned in (4) is located upshear, the maximum rainfall produced is three times that of when the newer cell is located downshear of the older cell.

(6) Two interacting clouds produce more rainfall than the single cloud.

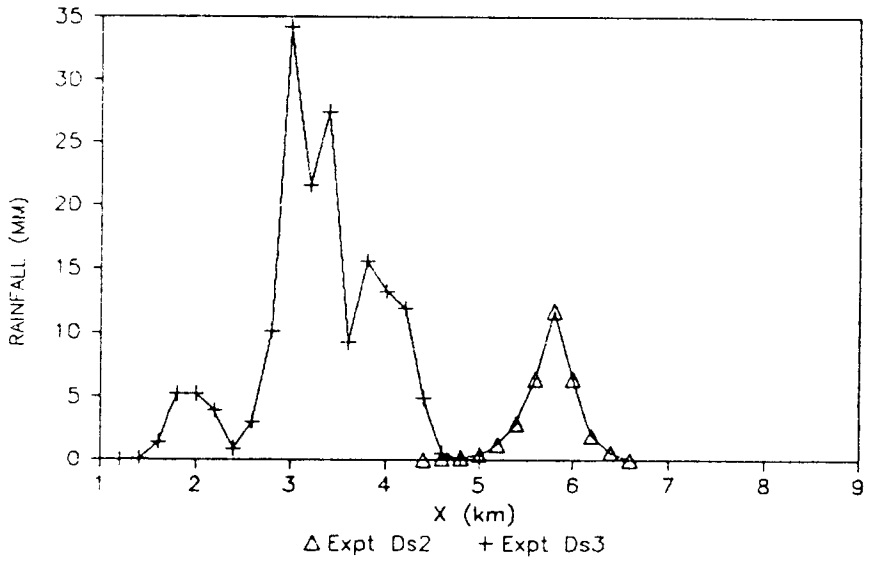

Fig. 11. Accumulated rainfall of Experiments Ds2 and Ds3.

There is however one feature in our results which somewhat differs from the previous studies. In comparison to other studies, our numerical simulations gave more rapid formation of rainfall which lasted about 10 to 15 minutes. This difference may be due to the following factors: (1) our model uses two top-hat temperature and buoyancy impulses to trigger cloud growth and (2) we use detailed microphysics wherein the droplets are categorized into 37 size classes.

6. Summary and conclusions

In this study, we develop a model for studying isolated cloud and double clouds. The model is 2-dimensional, slab-symmetric with detailed cloud physical processes. The model incorporates 37 classes of droplet sizes ranging from 1 μm to 4 mm radius. The growth of each droplet is governed by the use of detailed condensation and coalescence equations. Breakup is not included. We have applied the model to study the interactions of two cells in both calm and sheared environment.

In general, the results of the experiments show that the model is capable of simulating the general features of isolated, warm cloud development and rainfall. The structure and behavior of the model clouds appear to be in general agreement with the observations of Day 261 of GATE when small-size to moderate-size cumulus clouds developed in a southerly flow in the domain. The maximum height of the simulated, isolated cloud is 2.2 km under the same shear conditions, while typical observations ranged from 2 to 3 km. The lifetime of the model cloud is 30 minutes, attaining its peak development at 15-20 minutes which is the range for typical maritime clouds.

With regards to the simulation studies on cloud interactions the results indicated that merging occurred only when the model was initialized under calm environment. No merging occurred under sheared flow. In the case when the two identical cells were introduced simultaneously, the upshear cell developed while the growth of the downshear cell was suppressed. This is caused by the flow of moist air from the lower portion of the downshear cell towards the upshear cell.

Simulation studies were also carried out using non-simultaneous initial impulses. The younger cell grows at the expense of the older cell, irrespective of whether it is located downshear or

upshear of the older cell. However, the lifetime is longer and rainfall heavier when the newer cell is located upshear than when it is located downshear.

It is difficult to assess whether the results of our model, which has detailed microphysics, are more realistic than those that have been made with "bulk water" parameterization schemes, particularly in 3-d models. This assessment can be done in the future when adequate observations become available. However, it may be noted that our simulations with detailed microphysics give more rapid formation of rainfall as compared to simulations using bulk-water parameterization.

On the other hand, the advantage of the present model is that it can be used in the simulation of warm cloud seeding experiments. In this connection, it may be noted that several countries, e.g. Thailand, have operational rain enhancement programs which use warm cloud seeding techniques. We feel that our model can serve as a framework for testing the effects of artificial cloud seeding.

LIST OF SYMBOLS

Notation	Description	Value	Unit
a	Effect of surface tension on rate of condensation		cm
C	condensation or evaporation rate		$g\ kg^{-1}s^{-1}$
C_P	specific heat of air at constant pressure	1.004×10^{10}	$ergs\ kg^{-1}K^{-1}$
D	diffusion coefficient of water vapor	0.24	cm^2s^{-1}
$E(r,\ r')$	collection efficiency		cm^{-3}
e_s	saturation vapor pressure		mb
f	ventilation factor		
g	acceleration due to gravity	9.8	$m\ s^{-2}$
k	thermal conductivity of air	2411	$ergs\ cm^{-1}s^{-1}K^{-1}$
K	collection kernel		$cm^3\ s^{-1}$
L	latent energy of vaporization of water		$erg\ g^{-1}$
ℓ	liquid water content		$kg\ m^{-3}$
N	number of water droplets of each size per unit volume of air		cm^{-3}
q	mixing ratio of water vapor		$g\ kg^{-1}$
q_s	saturation mixing ratio of water vapor		$g\ kg^{-1}$
$R(J,\ J')$	redistribution factor		
Re	Reynolds number		
R_v	gas constant of water vapor	4.615×10^6	$ergs\ g^{-1}\ K^{-1}$
r	radius of droplet		cm
r_o	smallest radius of droplet considered in the model	.0001	cm
S	supersaturation		
T	temperature		K
T_v	virtual temperature		K
t	time		s
u	horizontal velocity		$m\ s^{-1}$
v	volume of droplet		cm^3
V_T	terminal velocity		$cm\ s^{-1}$
w	vertical velocity		$m\ s^{-1}$
x	mass of water droplet *also*, horizontal distance		g m

x_o	mass of droplet of radius 1μm		g
z	vertical distance		m
Γ_d	dry adiabatic lapse rate		K m^{-1}
ε	ratio of molecular weight of water to dry air	0.622	
ζ	vorticity		kg m^{-3} s^{-1}
η	number concentration of previously active nuclei		cm^{-3}
η^*	number concentration of active condensation nuclei		cm^{-3}
ρ_o	horizontal average of dry air density in initial field		kg m^{-3}
ρ_w	density of liquid water		kg cm^{-3}
σ	surface tension		
υ	eddy diffusion coefficient	25	m^2 s^{-1}
ψ	streamfunction		kg m^{-1} s^{-1}

REFERENCES

Byers, H. R. and R. R. Braham, Jr., 1949. The Thunderstorm: Report of the Thunderstorm Project. U. S. Goverment Printing Office, Washington D. C., 287 pp.

Gunn, R. and G. D. Kinzer, 1949. The terminal velocity of fall for water droplets in stagnant air. *J. Meteor.*, **6**, 243-248.

Hall, W. D., 1980. A detailed microphysical model within a two-dimensional dynamic framework model description and preliminary results. *J. Atmos. Sci.*, **37**, 2486-2507.

Kessler, E., 1969. On the Distribution and Continuity of Water Substance in Atmospheric Circulation. *Meteor. Mongr.* No. **32**, Amer. Meteor. Soc., 84 pp.

Lopez, R. E., 1976. Radar characteristics of the cloud populations of tropical disturbances in the northwest Atlantic. *Mon. Wea. Rev.*, **104**, 268-283.

Malkus, J. S., 1954. Some results of a trade-cumulus cloud investigation. *J. Meteor.*, **11**, 220-237.

Orville, H. D., 1965. A numerical study of the initiation of cumulus clouds over mountainous terrain. *J. Atmos Sci.*, **22**, 684-699.

Orville, H. D. and L. J. Sloan, 1970. A numerical simulation of the life history of a rainstorm. *J. Atmos. Sci.*, **27**, 1148-1159.

Orville, H. D. and F. J. Kopp, 1977. Numerical simulation of the life history of a hailstorm. *J. Atmos. Sci.*, **34**, 1596-1616.

Orville, H. D., Y. H. Kuo, R. D. Farley and C. S. Hwang, 1980. Numerical simulation of cloud interactions. *J. Rech. Atmos.*, **14**, 499-516.

Pruppacher, H. R. and J. D. Klett, 1980. Microphysics of clouds and precipitation. B. Reidel Publ. Con. Boston. 714 pp.

Scorer, R. S. and F. H. Ludlam, 1953. Bubble theory of penetrative convection. *Quart. J. Roy. Meteor. Soc.*, **79**, 94-103.

Simpson, J. M., 1980. Downdrafts as linkages on dynamic cumulus seeding effects, *J. Appl. Met.*, **19**, 477-487.

Simpson, J. M., W. L. Woodley, A. H. Miller and G. F. Cotton, 1971. Precipitation results of two randomized pyrotechnic seeding experiments. *J. Appl. Met.*, **10**, 526-544.

Takeda, T., 1971. Numerical simulation of a precipitating convective cloud: the formation of a "long-lasting" cloud. *J. Atmos. Sci.*, **28**, 350-376.

Tao, W. K. and J. Simpson, 1984. Cloud Interactions and Merging: Numerical Simulations. *J. Atmos. Sci.*, **41**, 2901-2917.

Turpeinen, O., 1982. Cloud interactions and merging on Day 261 of GATE. *Mon. Wea. Rev.*, **110**, 1238-1254.

Turpeinen, O. and M. K. Yau, 1981. Comparison of results from a three-dimensional cloud model with statistics of radar echoes on Day 261 of GATE. *Mon. Wea. Rev.*, **109**, 1495-1515.

Westcott, N. E., 1977. Radar characteristics of south Florida convective rainfall. M. S. thesis, Department of Env. Sciences, University of Virginia, Charlottesville, 74 pp.

Wilkins, E. M., Y. K. Sasaki, G. E. Gerber and W. H. Chaplin, Jr., 1976. Numerical simulations of the lateral interaction between buoyand clouds. *J. Atmos. Sci.*, **33**, 1321-1329.